PARYLENE-BASED ELECTROCHEMICAL-MEMS FORCE SENSOR ARRAY FOR ASSESSING NEURAL PROBE INSERTION MECHANICS

Brian J. Kim[1], Christian A. Gutierrez[1], Greg A. Gerhardt[2], and Ellis Meng[1]
[1]University of Southern California, Los Angeles, CA, USA
[2]University of Kentucky Chandler School of Medicine, Lexington, KY, USA

ABSTRACT

We present the first use of a Parylene-based electrochemical-MEMS (EC-MEMS) sensor array for instrumentation of ceramic-based neural electrode probes. The sensor array consists of a liquid-filled Parylene-based microchannel and an array of enclosed electrodes that monitor local variations in impedance during mechanical deformation of the channel. The array provides real time measurement of out-of-plane interfacial forces produced directly on the electrode shank surface (<5 mm^2) during insertion of the probe. We demonstrate the ability to examine the relative force distribution of interfacial forces produced on the shank surface during insertion, thereby providing a clearer understanding of probe insertion mechanics. Our approach enables, for the first time, robust mechanical instrumentation of electrode shanks providing a means for assessing the poorly understood interfacial mechanics between neural probes and tissue.

INTRODUCTION

Current designs of implantable neural probes for neuronal recording and stimulation largely ignore mechanical considerations, which may contribute to limited performance and lifetime *in vivo*. Understanding the link between insertion-induced mechanical damage and electrode shank design is necessary to guide the design of next generation probes, such that tissue damage and the related immunological responses are minimized [1]. Instrumentation of the electrode surface with tiny physical sensors captures important mechanical interactions between the probe and tissue that impact probe shape, material, and insertion parameters.

Previously, external load cells were used to measure macroscale insertion forces [2], but limited insight into interfacial phenomena was gained and out-of-plane stresses acting on the shank surface could not be detected. Recently, CMOS sensors integrated on a silicon shank were used to measure interfacial stresses [3]. This design, however, was limited to measurement of stresses in the bulk material and only compatible with silicon-based neural probes. A more versatile approach is necessary to enable comparative studies between different electrode designs and materials. Sensors must be able to: accommodate small shank areas, integrate with CMOS-incompatible electrode shank materials, and operate in aqueous and high salt environments. To address this unmet need, we adapted our Parylene-based EC-MEMS sensing technology to transduce force and pressure distributions directly on the electrode shank surface [4]. We present a new sensor layout capable of integration directly onto existing implantable ceramic electrode shanks [5] and demonstrate, for the first time, the relative force distribution produced along the shank surface in agarose tissue phantoms.

DESIGN AND OPERATION

The linear array of seven sensors is constructed on a flexible Parylene C substrate and within a Parylene C microchannel (100 µm width, 4.5 mm length) that serves as a contact surface. Platinum microelectrodes (2000 Å thick) exposed to the fluidic contents of the channel interior provide an electrical interface for electrochemical impedance measurements; pairs of adjacent electrodes form sensor units (Figure 1). Etched fluidic ports at channel ends allow the surrounding electrolyte to fill the channel. Fluid can flow freely between the external environment and the channel via the access ports.
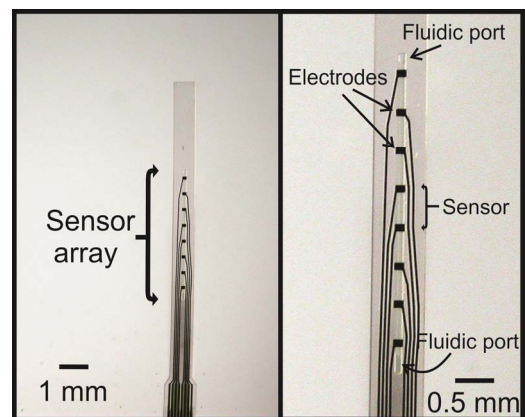

Figure 1: Optical micrograph of Parylene force sensor array (100 µm width, 4.5 mm length, and 20 µm height). Magnified view illustrates the layout of the thin film platinum electrodes and the position of the fluidic ports.
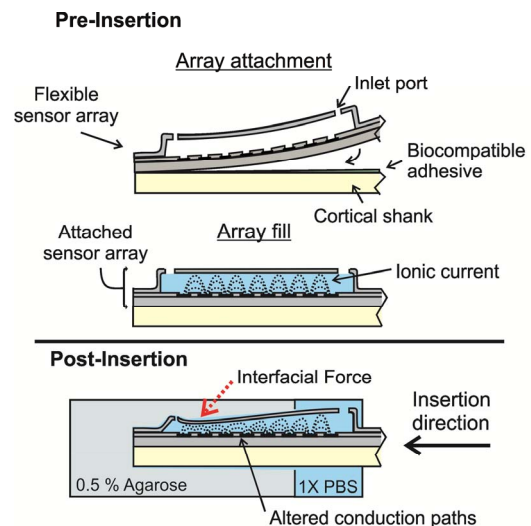

Figure 2: Illustration depicting transduction method of the sensor array. Prior to insertion, the ionic current remains undisturbed between electrodes. Insertion into agarose (tissue phantom) results in interfacial forces that deform the channel and changes sensor impedance.

During insertion, external contact forces deform the compliant fluid-filled structure in the normal direction and redistribute the fluid contained within the chamber. Changes to the ionic conduction path of current-carrying ions in the fluid register as a change in the magnitude of the solution impedance (Figure 2). Thus, impedance variations can be correlated to mechanical interfacial contact forces exerted by the tissue in contact with the top of the sensor array.

EXPERIMENTAL METHODS

Fabrication

Standard surface micromachining processes were used for sensor array fabrication (Figure 3). All fabrication processes were performed at low temperatures (90 °C) to prevent excessive thermal cycling of the Parylene C structural material. Parylene C was chosen as the sensor material for its biocompatibility, mechanical strength, electrical insulation properties, and ability to form pinhole free films via chemical vapor deposition at room temperature.

Platinum electrodes and contact pads (2000 Å) were patterned by lift-off on a Parylene substrate (5 µm) coated onto a silicon carrier wafer. Following deposition of a Parylene insulation layer (1.5 µm), openings for electrodes and contact pads were etched using oxygen plasma. A 20 µm high sacrificial photoresist layer was spun-on to form the structure for the microchannel sensing element, and a 4 µm thick layer of Parylene was deposited to form the final device structure. Fluidic access ports at the channel ends were opened by oxygen plasma. Finally, to facilitate precise shaping of the array for attachment to a fine ceramic shank tip, arrays were cut out using a switched chemistry (C_4F_8 and O_2 plasma) etching process [6].
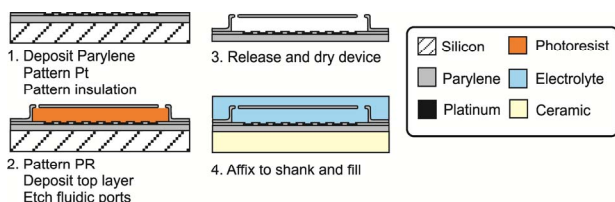

Figure 3: Abbreviated process flow for array fabrication and attachment utilizing standard surface micromachining techniques. Cross-section taken laterally through device microchannel.

Devices were released from the wafer by stripping the protective photoresist mask for the cut-out etch, and then submerging the wafer in DI water. The hydrophobicity of the Parylene polymer allowed the arrays to easily separate from the silicon wafer and lift-off the surface. Sacrificial photoresist was then removed by immersion in acetone and isopropyl alcohol and arrays were dried (Figure 4).

Array Packaging

Prior to attachment to ceramic shank tips, arrays were first electrically packaged to a zero-insertion force (ZIF) connector (Hirose 8 channel, 0.5 mm pitch) (Figure 5a). Details of the epoxy-less, ZIF connection scheme for Parylene cables are described in our prior work [7]. Briefly; a PEEK stiffener was attached to the contact pad end to allow for proper connection with a custom ZIF-ZIF adaptor connector. The adaptor facilitated connection to a commercially available flat flexible cable that enabled integration with the rest of the test system.
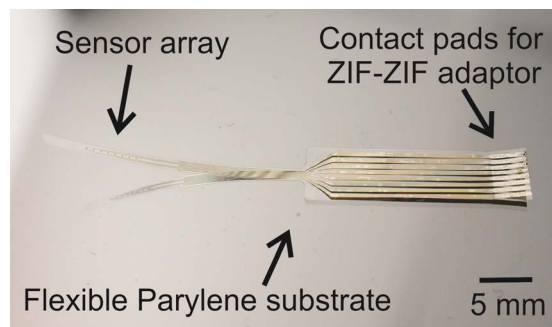

Figure 4: Released sensor array prior to attachment to shank. Integrated contact pads allow simple, solder-less, and repeatable connections via a ZIF connector.

Packaged arrays were adhered to the ceramic electrode shank tip using a thin layer of biocompatible superglue (Adhesive Systems MG 100 USP Class VI) (Figure 5b).
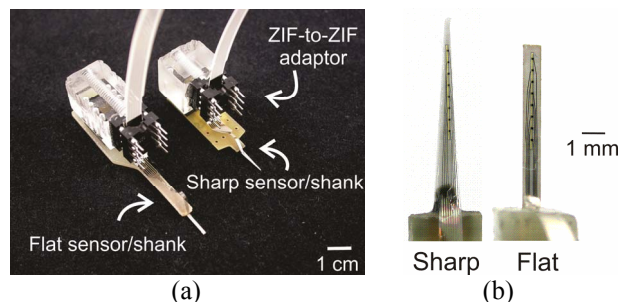

Figure 5: a) Instrumented ceramic electrode shanks in acrylic jigs for insertion experiments. The white flat flexible cables connect to a ZIF connector on a custom PCB. b) Optical micrograph of the sensor array affixed to two different ceramic electrode shank designs.

Biocompatible adhesive was chosen to minimize immunological responses to the instrumented shank. The superglue is soluble in acetone so that sensors can be removed from the ceramic shanks, allowing reuse of electrodes. For *in vitro* testing, instrumented ceramic electrode shanks were interfaced to an acrylic test jig, which allowed attachment to the insertion setup (Figure 5a).

Experimental Setup

Insertion experiments were conducted into agarose phantom models of cortical tissue (0.5%) in a bath of 1× phosphate buffered saline (PBS) to mimic wet, *in vivo* conditions. The setup consisted of the acrylic jig attached to a 50 g load cell, for normal insertion force measurements, all affixed to a motorized micropositioning stage that controlled insertion speed and depth into the tissue phantom. Impedance was measured by a LabVIEW-interfaced precision LCR meter (1 V_{p-p} sinusoid, 10 kHz) via a multiplexing PCB for multi-channel impedance measurement across the seven sensors of the array. Electrochemical impedance spectroscopy (EIS) yielded 10 kHz as the optimum frequency to

measure solution impedance to minimize system phase (Figure 6). The motorized stage, LCR meter, and PCB digital switching all interfaced with LabVIEW to give the user control of insertion speed and depth as well as a real-time image (graphical) of the impedance changes (interfacial forces) across the ceramic electrode shank.
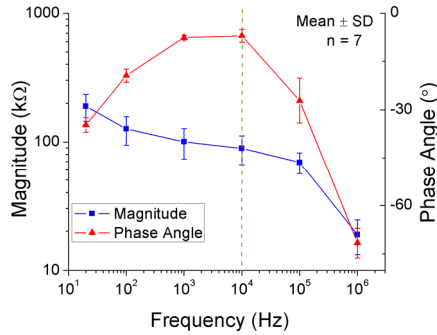

Figure 6: EIS magnitude and phase plots for sensor electrodes. 10 kHz was chosen to bypass capacitive effects at the electrode-electrolyte interface and maximize solution impedance (phase of ~0°).

Prior to insertion experiments, sensor arrays were filled via immersion with $1\times$ PBS electrolyte following a short immersion in isopropyl alcohol (a Parylene wetting step to facilitate diffusion of the polar PBS into the microchannel). Instrumented ceramic electrode shanks were inserted 3.5 mm (Figure 7) into agarose at three different speeds: 0.01 mm/s (slow), 0.03 mm/s (medium), and 0.1 mm/s (fast), held at the maximum displacement for five minutes, and extracted at the same speed.
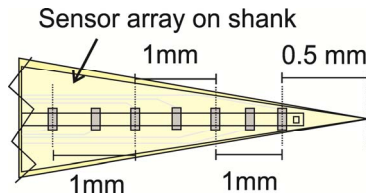

Figure 7: Spacing of sensor array on a sharp ceramic electrode shank. A displacement of 3.5 mm into agarose covers up to 6 sensors of the array.

RESULTS AND DISCUSSION
Normal Insertion Forces

Normal neural probe insertion forces were reported by others, but are briefly mentioned here to provide a complete picture of insertion mechanics. There are two main forces that dominate mechanics during probe insertion: tissue displacement forces enacted by the shank on tissue and frictional forces caused by the shank tip moving through tissue [1]. Measurements of normal insertion forces combine these two phenomena into a single measurement to provide unclear information on insertion mechanics. We observed that with increasing insertion speeds, the normal insertion forces increase: with forces nearly doubling with a 10× increase in speed (Table 1). We hypothesize that this is due to the increased resistance to insertion by the tissue that is encountered with increases in insertion speed.
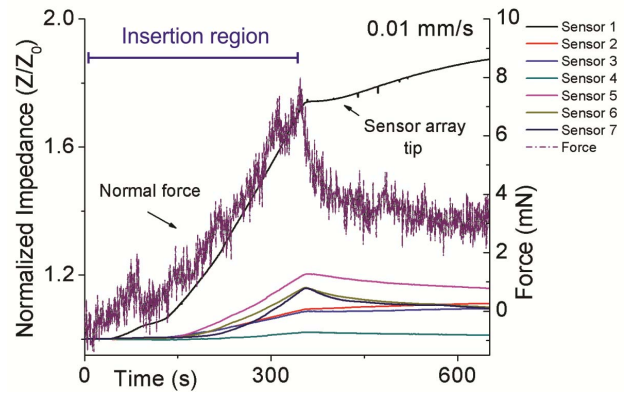

Figure 8: Representative plot of insertion experiments (sharp electrode shank design at the 0.01 mm/s insertion speed). Normal insertion forces are in purple. Plot shows the insertion of instrumented ceramic electrode shanks into agarose with a 5 minute hold at the maximum displacement (3.5 mm).

Table 1: Summary of agarose insertion experiments of the sharp shank design for three insertion speeds.

Speed (mm/s)	Maximum normal force (mN)	Maximum ΔZ% : Sensor 1 (shank tip)	Average maximum ΔZ % change: Sensors 2-7 (n=6, mean ± SE)
0.01	7.99	87 %	12 ± 3%
0.03	8.94	38 %	2 ± 1%
0.1	15.60	28 %	1 ± 0.6%

Shank Interfacial Forces

By correlating the magnitude of impedance changes (normalized) to a force magnitude, we are able to obtain comparisons of the relative magnitudes of forces that are experienced across the ceramic electrode tip. Initial finite element modeling results indicate that the force range that can be measured with this device geometry is in the range of tens of milli-Newtons (up to 60 mN for a near maximum 18 μm chamber deflection).

Noting that sensors 1-7 begin at the shank tip and move to its base, data indicate that a majority of the interfacial forces during insertion are within the first millimeter of the electrode shank (the first sensor; Figure 8). This is also evidenced by the results across all three insertion speeds; the maximum percentage impedance change of the first sensor is considerably higher than that of the remaining sensors higher up on the shank (Table 1). We attribute the interfacial forces experienced at the tip during insertion to the tissue displacement and propagation of the electrode shank track generated by the probe. Additional force is imposed by tissue as it is being displaced during insertion.

In varying insertion speed, we also observed that the interfacial forces at the shank tip (first millimeter) decrease as the speed increases. In analyzing this phenomenon we must also consider the effects of frictional forces exhibited by the electrode shank during insertion. Slower insertion speeds allow for a longer travel time through tissue, increasing shank-tissue adhesion and thus the frictional forces between the shank and tissue. Results confirm that faster speeds decrease the interfacial forces experienced at the tip (by tissue

displacement and frictional forces) [1] as the max percentage impedance change is lower by nearly 60% (Table 1).

This effect of speed on interfacial forces is consistent throughout the length of the shank. At the slowest speed, increased frictional forces resulting in additional array deformation during insertion give rise to higher average impedance change in other sensors; Sensors 2-7 recorded an average maximum percentage impedance change of 12% compared to 2% and 1% at the medium and fast speeds, respectively. Therefore, faster speeds also reduce adhesion forces between the shank and surrounding tissue along the length of the tip.

In summary, a mechanics analysis limited to normal insertion forces might suggest that slower insertion speeds benefit insertion by decreasing the forces encountered during probe implantation. However, before this conclusion can be made, it is also important to consider interfacial forces and the effects of tissue displacement and frictional forces; faster insertion speeds not only reduce the forces at the shank tip created during insertion, but also the frictional forces observed. Measurement of interfacial forces elucidates the locations and magnitudes of tissue displacement and frictional forces during insertion.

Force ranges and sensitivity for a particular EC-MEMS force sensor can be tuned by changes in device geometry and thickness to accommodate interfacial force ranges expected during insertion. Currently, further characterization of the sensor array to obtain a calibration curve between force and impedance change is underway.

Micromotion

Electrode shank instrumentation also provides the benefit of additional sensing capabilities. More specifically, it has been reported that micromotion of the brain occurs during craniectomies due to pulsed blood flow and respiration [8]. Micromotion events can affect implanted probes and result in disrupted recording due to positional changes. We also demonstrate the ability to detect micromotion events such that sensory feedback can be used to distinguish neural signals from micromotion events (Figure 9).
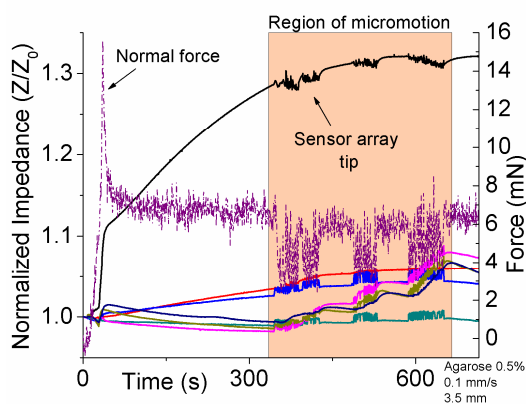

Figure 9: Results from simulated micromotion experiments. Micromotion was produced by displacing the agarose substrate ±1 mm normal to shank face. Highlighted region contains 3 micromotion events.

CONCLUSION

We designed, fabricated, and tested a Parylene-based EC-MEMS sensor array for instrumentation of a ceramic electrode shank. We demonstrated the ability to track the relative distribution of interfacial forces produced along the shank surface during insertion. We determined that interfacial forces primarily act on the first millimeter of the shank which imposes a significant portion of the tissue displacement forces, and that faster insertion speeds reduce interfacial forces experienced along the shank tip. We also demonstrated tracking of micromotion in implanted neural probes. Following additional characterization, *in vivo* studies with instrumented shanks will be performed to gain a more complete understanding of insertion mechanics.

ACKNOWLEDGEMENTS

REFERENCES

[1] A. A. Sharp, *et al.*, "In Vivo Penetration Mechanics and Mechanical Properties of Mouse Brain Tissue at Micrometer Scales," *Biomedical Engineering, IEEE Transactions on,* vol. 56, pp. 45-53, 2009.

[2] R. Hoffmann, *et al.*, "Comparative Study on the Insertion Behavior of Cerebral Microprobes," in *Engineering in Medicine and Biology Society, 2007. EMBS 2007. 29th Annual International Conference of the IEEE*, 2007, pp. 4711-4714.

[3] K. Seidl, *et al.*, "CMOS-based high-density silicon microprobe for stress mapping in intracortical applications," in *Micro Electro Mechanical Systems (MEMS), 2010 IEEE 23rd International Conference on*, 2010, pp. 35-38.

[4] C. A. Gutierrez and E. Meng, "Impedance-Based Force Transduction Within Fluid-Filled Parylene Microstructures," *Journal of Microelectromechanical Systems,* vol. 20, pp. 1098-1108, Oct 2011.

[5] J. J. Burmeister, *et al.*, "Ceramic-based multisite microelectrodes for electrochemical recordings," *Analytical Chemistry,* vol. 72, pp. 187-192, Jan 1 2000.

[6] E. Meng, *et al.*, "Plasma removal of parylene c," *Journal of Micromechanics and Microengineering,* vol. 18, Apr 2008.

[7] C. A. Gutierrez, *et al.*, "Epoxy-less packaging methods for electrical contact to parylene-based flat flexible cables," in *Solid-State Sensors, Actuators and Microsystems Conference (TRANSDUCERS), 2011 16th International*, 2011, pp. 2299-2302.

[8] L. Xindong, *et al.*, "Stability of the interface between neural tissue and chronically implanted intracortical microelectrodes," *Rehabilitation Engineering, IEEE Transactions on,* vol. 7, pp. 315-326, 1999.

CONTACT

*B.J. Kim, tel: +1-213-8213949; brianjk@usc.edu